Systemic inflammation triggers long-lasting neuroinflammation and accelerates neurodegeneration in a rat model of Parkinson's disease overexpressing human α-synuclein

Mariangela Massaro Cenere[1,2,3 *], Marta Tiberi[2,4], Emanuela Paldino[5], Sebastian Luca D'Addario[1,3], Mauro Federici[1], Cecilia Giacomet[1,2,3], Debora Cutuli[1,6], Alessandro Matteocci[4,7], Francesca Cossa[1,2,3], Beatrice Zarrilli[1,2,3], Ada Ledonne[1,2,3], Laura Petrosini[1], Nicola Berretta[1,3], Francesca Romana Fusco[5], Valerio Chiurchiù[4,8 #], Nicola B. Mercuri[1,2,3#]

[1]*Department of Experimental Neuroscience, Santa Lucia Foundation IRCCS, Rome, Italy;*

[2]*Department of Systems Medicine, University of Rome Tor Vergata, Rome, Italy;*

[3]*Aligning Science Across Parkinson's (ASAP) Collaborative Research Network, Chevy Chase, MD, United States*

[4]*Laboratory of Resolution of Neuroinflammation, Santa Lucia Foundation IRCCS, Rome, Italy;*

[5]*Laboratory of Neuroanatomy, Santa Lucia Foundation IRCCS, Rome, Italy;*

[6]*Department of Psychology, Sapienza University of Rome, Rome, Italy;*

[7]*PhD program in Immunology, Molecular Medicine and Applied biotechnologies, University of Rome Tor Vergata, 00133 Rome, Italy;*

[8]*Institute of Translational Pharmacology, National Research Council, Rome, Italy.*

*Correspondence to: mariangela.massarocenere@gmail.com, mercurin@med.uniroma2.it

[#]Equally senior authors

ABSTRACT

Increasing efforts have been made to elucidate how genetic and environmental factors interact in Parkinson's disease (PD). In the present study, we assessed the development of PD-like symptoms on a genetic PD rat model overexpressing human α-synuclein (*Snca*$^{+/+}$) at a presymptomatic age, exposed to a pro-inflammatory insult by intraperitoneal injection of lipopolysaccharide (LPS), using immunohistology, high-dimensional flow cytometry, electrophysiology, and behavioral analyses. A single injection of LPS to both WT and *Snca*$^{+/+}$ rats triggered long-lasting increased activation of pro-inflammatory microglial markers, infiltrating monocytes and T-lymphocytes. However, only LPS *Snca*$^{+/+}$ rats displayed dopaminergic neuronal loss in the *substantia nigra pars compacta* (SNpc), associated with a reduction of evoked dopamine release in the striatum. No significant changes were observed in the behavioral domain.

We propose our double-hit animal as a reliable model to investigate the mechanisms whereby α-synuclein and inflammation interact to promote neurodegeneration in PD.

INTRODUCTION

Parkinson's disease (PD) is a progressive neurodegenerative pathology affecting more than 7 million people worldwide [1]. It is characterized by motor symptoms (such as bradykinesia, rigidity, resting tremor, and postural instability) and non-motor symptoms (lack of motivation, anxiety, dementia, depression, hallucinations, sleep disorders, pain, and gastrointestinal dysfunction) [2–4]. The main pathological hallmarks of PD are a slow and progressive loss of dopaminergic (DAergic) neurons in the *substantia nigra pars compacta* (SNpc), causing decreased synaptic outflow of DA in the striatum, and accumulation of misfolded neuronal α-synuclein inclusions, known as Lewy bodies (LBs) and Lewy neurites (LNs) [4–6].

Most cases of PD are sporadic. However, genome-wide association studies (GWAS) have identified over 90 genetic risk loci [7], responsible for an overall heritable component of the disease estimated at around 35% [8]. Missense mutations and overexpression of the α-synuclein gene (*Snca*), one of the most common mutations in monogenic PD, are widely used to model PD in rodents; however, no single animal model replicates all pathogenic and clinical PD features, and some of them fail to develop nigral DAergic neurodegeneration. Hence, there is common agreement that environmental factors significantly contribute to PD pathogenesis. Indeed, it is worth noting that patients exhibiting the same genetic mutation may not have analogous clinical presentations, suggesting that a complex interaction exists among environmental, age-associated, and genetic factors responsible for the aetiology of the disease [9,10].

It has been proposed that endotoxins may participate in PD pathogenesis [11]. The lipopolysaccharide (LPS) is the most used endotoxin to elicit an acute immune response. It is a major component of the outer membrane of gram-negative bacteria and a potent inducer of inflammation in peripheral tissues and the central nervous system via activation of toll-like receptor 4 (TLR4). Multiple studies support LPS treatment as an experimental model to reproduce PD-like symptoms in the animal. Progressive DAergic neurons' degeneration and glial cell activation are reported following LPS intraperitoneal (i.p.) injection in *wild-type* animals [12–15]. Repeated i.p. injections of LPS over four consecutive days in 3-month-old male mice triggered a reduction in the number of SNpc tyrosine hydroxylase-positive (TH^+) and NeuN-positive neurons 19 days after the first LPS injection [15]; however, no further cellular reduction was found at 36 days post-injection [16]. The shift in cytokine production, with increased anti-inflammatory and reduced pro-inflammatory cytokines, indicates that, at later stages, animals develop cellular and molecular strategies to stop the ongoing neurodegenerative process [16]. In line with this, TH protein levels decreased in the SN of Wistar rats 15 days after a single dose of LPS, followed by recovery 30 and 60 days post-injection [17].

In the present investigation, we tested the hypothesis that PD development occurs through a double-hit mechanism involving the combined interplay of elevated endotoxin and aggregated α-synuclein, with the outcome of neuronal degeneration in the SNpc. To this aim, we used rats overexpressing human α-synuclein (*Snca*$^{+/+}$) characterized by a prodromal asymptomatic phase, with the first functional signs of DAergic pathology starting at four months of age, later resulting in a 25-27% depletion of TH and soma-dendritic neuronal modification at 12 months, accompanied by altered firing properties of DAergic neurons [18–21]. In this animal model, we induced systemic inflammation at a presymptomatic age (2 months) via a single intraperitoneal injection of LPS, and we evaluated the effects on neuroinflammation and the DAergic system three months later.

RESULTS

Time course of sickness behavior and body weight

Since LPS stimulates the release of several pro-inflammatory cytokines that are associated with fever, sickness behavior, and body weight loss [22,23], we first measured sickness signs and body weight over time (2h, 18h, 24h, 42h, 48h, 72h, 96h, and 168h) after LPS i.p. injection (Supplementary Fig. 1A-D). No sickness signs were observed in saline (SAL)-treated WT and *Snca*$^{+/+}$ rats except for slightly decreased exploration and locomotor activity in 10% of *Snca*$^{+/+}$ rats (score =2) 24h after saline injection. The LPS-treated groups exhibited clear signs of sickness compared to controls. The maximum score was reached at 24h, when rats manifested decreased locomotion and explorative behavior, curled body posture, closed eyes, piloerection, and irregular fur (Supplementary Fig.1 A, B). SAL *Snca*$^{+/+}$ rats increased their body weight by 20 g ± 6 g over seven days, whereas LPS injection resulted in acute weight loss. Post hoc analysis demonstrated that LPS *Snca*$^{+/+}$ rats lost weight in the first 72h compared with SAL-treated rats, decreasing their body weight by 42 g ± 5 g at 18h and then gradually recovering weight during the following weeks (Supplementary Fig.1 C, D).

Effects of peripheral LPS on long-lasting neuroinflammation

We next sought to investigate whether a single systemic dose of LPS injection was sufficient to elicit long-lasting inflammation in both SNpc and striatum, by using the sophisticated approach of high dimensional flow cytometry, enabling us to identify all the different brain resident and infiltrated immune cells (Fig. 1A).

We observed that the percentage of CD45^{high}CD11b^{high} infiltrated monocytes/macrophages was higher in *Snca*$^{+/+}$ rats compared with WT rats, both in the SNpc and the striatum. This percentage was even higher in LPS-treated groups, especially *Snca*$^{+/+}$ rats (Fig.1B).

On the other hand, no significant changes were observed in the percentage of the resident myeloid cells of the brain, *i.e.,* CD45^{low}CD11b^{+} microglia in the LPS-treated groups compared to the SAL-treated group (Fig.1C). Similar results were obtained with unbiased stereological cell count; no significant increase in the number of IBA1^{+} cells was found in the SNpc and the striatum of LPS *Snca*$^{+/+}$ compared with SAL *Snca*$^{+/+}$ rats (Supplementary Fig.2A-B).

Although microglial cell count did not change, we next sought to further characterize the activation state of CD45^{low}CD11b^{+} microglia by assessing the expression of pro-inflammatory M1-like markers CD86 and MHC-II (Fig.1D). In WT rats, CD86 was not significantly altered in the two brain regions at three months after LPS administration (Fig.1D). MHC-II was significantly increased in the LPS WT group compared to the SAL-treated groups in the SNpc (Fig.1E, top) but

not in the striatum (Fig.1E, bottom). On the other hand, expression levels of CD86 were significantly higher in *Snca*$^{+/+}$ rats in both SNpc and striatum regardless of the treatment and were even higher upon LPS stimulation (Fig.1D). In contrast, the levels of MHC-II were increased in the *Snca*$^{+/+}$ rats compared to WT rats only in the SNpc (Fig.1E, top) and such levels were even higher following LPS treatment in both brain areas (Fig.1E).

Since microglia's resting/activation state is associated with its morphological changes, we next performed a Sholl analysis of IBA1^{+} cells. Notably, microglia displayed a decreased complexity, shorter branching, decreased number of intersections, endings, and nodes in LPS *Snca*$^{+/+}$ compared with the SAL-treated group in SNpc and striatum (Supplementary Fig. 2 E-F).

These data proved that a single systemic LPS dose triggers a neuroinflammatory response in the SNpc and the striatum that likely involves microglia activation.

Effects of peripheral LPS on leukocyte infiltration

Given that peripheral-derived immune cells are also present in brain tissue and contribute to disease pathology [24], we investigated whether a single systemic LPS administration affects peripheral immune cell infiltration into the SNpc and the striatum. To this end, the rest of the CD45^{high}CD11b^{low} cells (Fig.1A) were further gated by high dimensional flow cytometry to identify CD3^{+} T-lymphocytes, CD45RA^{+} B-lymphocytes and CD161^{+} NK cells. We observed that only infiltrating T-lymphocytes were significantly increased in the SNpc of LPS *Snca*$^{+/+}$ rats compared to SAL- and LPS-treated WT rats (Fig.2A, top). No changes were found in the percentage of infiltrating B-lymphocytes and NK cells (Fig.2B-C). On the other hand, in the striatum, increased percentages of T-lymphocytes were also observed in WT rats upon LPS treatment (Fig.2A, bottom), along with a significant increase in infiltrating NK cells in *Snca*$^{+/+}$ rats compared with WT rats, but not following LPS treatment (Fig.2C, bottom panel). Since we reported an increase in T lymphocytes within the brain of *Snca*$^{+/+}$ rats and recent evidence supports a key role for T cells in PD pathogenesis [25], we further investigated the immunophenotype of peripheral blood mononuclear cells (PBMCs) (Supplementary Fig.3A) to assess whether differences of immune infiltrates reflect changes in the peripheral blood. No significant changes were observed in the percentage of B cells (Supplementary Fig.3B), NK cells (Supplementary Fig.3C), and granulocytes (Supplementary Fig.3D). At the same time monocytes were higher only in LPS *Snca*$^{+/+}$ rats compared to the other experimental groups (Supplementary Fig.3E). Interestingly, the proportion of T cells was significantly increased in both genotypes following LPS stimulation (Supplementary Fig.3F).

Effects of peripheral LPS on nigrostriatal alterations in Snca$^{+/+}$rats

To test the hypothesis that endotoxin may enhance nigral DAergic neuron degeneration in *Snca*$^{+/+}$ rats, we evaluated the immunohistological changes in nigral neurons three months after the injection via the unbiased stereological cell count, by staining midbrain coronal sections with TH as a DAergic marker.

The unbiased stereological count confirmed the absence of TH$^+$ neuronal loss in SAL *Snca*$^{+/+}$ compared to the SAL WT rats (Fig.3A), as previously reported [19]. Three months after a single LPS i.p. injection, both WT and *Snca*$^{+/+}$ groups showed a statistically significant decreased number of TH$^+$ neurons in the SNpc, by almost 28% (±7% SEM) and 49% (±8% SEM) compared to SAL WT rats (Fig.3A). Since a study by Heo and colleagues [26] demonstrated that some SNpc DAergic neurons could lose their TH expression and become so-called dormant neurons, we tested whether the observed decrease in TH$^+$ neurons in LPS-treated rats could reflect TH downregulation, rather than an actual neuronal loss, by using DOPA decarboxylase (DDC) as an additional DAergic marker. We found TH-negative (TH$^-$) neurons that were DDC-positive (DDC$^+$) mainly in LPS WT but not in the LPS *Snca*$^{+/+}$ rats (Fig.3B), indicating that in LPS WT rats some SNpc DAergic neurons lose their TH-phenotype, and could be surviving or bound to die neurons. In contrast an actual loss of TH$^+$ neurons only occurs in LPS *Snca*$^{+/+}$ rats.

SNpc DA neurons have extensive dendritic arborization that extends ventrally towards the SN pars reticulata (SNpr). In *Snca*$^{+/+}$ rats injected with LPS this TH$^+$ dendritic projection showed changes in morphology and density. Optical densitometry showed a significant loss of TH$^+$ dendrites at three months after LPS injection, compared to SAL-treated groups (Fig.3C). Dendrites from the remaining DAergic neurons appeared truncated with a distorted morphology (swollen and bubble-shaped) compared to the other experimental groups, where they showed a lengthened and smooth profile (Fig.3C).

The densitometric analysis of multiple sections of DAergic terminals in the dorsal striatum showed no significant decrease in TH immunoreactivity in LPS-treated rats compared with the SAL-treated groups, despite the decrease of SNpc TH$^+$ neurons and altered dendritic arborization (Fig.4D).

In addition, constant potential amperometry measurements of DA outflow in the dorsolateral striatum revealed a significant decrease of evoked DA amplitude in LPS *Snca*$^{+/+}$ rats compared with SAL-treated rats (Fig.4A), with no significant change in the half-decay time (192.7 ± 1.7 ms vs. 195.9 ± 1.9 ms, respectively). In previous studies in four-month-old naïve *Snca*$^{+/+}$ rats [19], we found a reduced DA outflow in the dorsal striatum in SAL *Snca*$^{+/+}$ compared with WT rats. Here, we found a more significant decrease in DA release when combining genetic and endotoxic risk factors.

No significant differences were found in LPS WT rats compared with SAL WT (Fig.4A) in either amplitude or half-decay.

Next, to further explore possible alterations of DA release, we analyzed the modifications of DA transporter (DAT) function in *Snca*$^{+/+}$ rats via superfusion of striatal coronal slices with the DAT blocker cocaine. As expected, cocaine (0.3-1 µM) increased the amplitude of the amperometric signal in a concentration-dependent manner and increased its half-decay time [27]. However, we did not find any significant difference between the two experimental groups either at low (0.3 µM) or high (1 µM) concentrations of cocaine (Fig.4B).

Additionally, we next investigated the function of DA autoreceptors (D2R) on DAergic transmission [28,29]. To this end, we superfused striatal slices with a low dose of the D2-agonist quinpirole (0.03 µM). As expected, quinpirole reduced evoked DA efflux by almost 30%; however, no difference was observed in quinpirole effect on the DA signal between SAL *Snca*$^{+/+}$ and LPS *Snca*$^{+/+}$ rats (Fig. 4C).

Possible functional alterations of the DAergic transmission were also evaluated by assessing the animal's general locomotor activity and depressive-like behavior via the rotarod and open field tests, and the sucrose preference test, respectively. No significant differences were observed in these behavioral tests in the animals three months after a single LPS dose (Supplementary Fig.4A-C). Since the two-way ANOVA revealed a significant treatment effect in the sucrose solution intake, we then performed Tukey's multiple comparison *post hoc* test; however, no difference was pointed out among the four experimental groups (Supplementary Fig.4C).

DISCUSSION

There is now a wide consensus that PD is a multisystem disorder involving genetic and environmental risk factors. However, understanding the complex mechanisms underlying gene and environment interactions presents a significant challenge. Our present data propose human α-synuclein expressing rats injected with LPS as a reliable model to investigate how these two factors cooperate in the genesis and progression of the neurodegenerative processes in the DAergic system typical of PD, pointing to inflammation as a connective element of this harmful cooperation.

A prodromal symptomatic phase usually characterizes PD animal models based on SNCA gene mutation and overexpression. Previously, we described the human α-synuclein overexpressing rat model, used in this study, showing a presymptomatic phase preceding early pathological signs occurring at four months. At this age, rats exhibit a significant reduction of striatal DA release despite the integrity of DAergic terminals and in the absence of nigral neuronal loss. These early alterations are paralleled by neuroinflammation in the CNS, with microglial activation and increased levels of pro-inflammatory cytokines in the cerebrospinal fluid (INFγ), while in the blood granulocytes, T, and B cells are not altered [19]. *Snca*$^{+/+}$ rats exhibit robust, long-lasting central and peripheral inflammatory activation when combined with an early event of acutely induced inflammation. Most notably, microglia were markedly activated, polarizing towards a more pro-inflammatory phenotype, and accompanied by monocyte and T-lymphocyte infiltration into the brain parenchyma. In contrast, LPS WT rats displayed mild differences from SAL-treated WT, with no macrophagic infiltration and only increased levels of microglia MHC-II pro-inflammatory activation markers in the SN and few infiltrating T-lymphocyte into the striatum.

Interestingly, enhanced nigral microgliosis was also reported in a transgenic mouse model expressing mutated α-synuclein, i.p. injected with LPS at the early symptomatic age [30]. This study shows a delayed chronic and progressive degeneration of nigral TH^{+} neurons, with a more prominent effect five months after LPS injection. The increased infiltration of T-lymphocytes into the brain parenchyma reported in the present study is of particular interest since T cells are known to play a key role in both the CNS and periphery, leading to a profound imbalance of the immune network in PD patients [31]. T lymphocytes were reported in postmortem brain specimens from PD patients [29,30] and a mouse model of PD [32]; additionally, CD4^{+} T cell knock-out on a PD mouse model resulted in a markedly reduced DAergic neuronal death [32]. These data strengthen the hypothesis that T cells are crucial for neurodegeneration during PD and support the contribution of autoimmune-based pathogenesis for this disease [25,31,32].

Since inflammation triggers neurodegeneration, we hypothesized that LPS could also affect DAergic neuron viability. Our findings show that LPS injection in *Snca*$^{+/+}$ rats significantly

degenerates the DAergic neurons. This was observed at an age (5 months) when these animals do not normally present signs of neurodegenerative processes in the SNpc. While the observed reduction of TH^+ neurons in both WT and *Snca*$^{+/+}$ rats takes place independently from α-synuclein, the decrease of DDC^+ neurons that only occurred in LPS *Snca*$^{+/+}$ rats suggests that the DAergic neuron death only happens in response to a double-hit of genetic human α-synuclein overexpression and endotoxin-induced inflammation. The decreased TH^+ neurons in LPS WT rats could reflect TH downregulation. Indeed, Heo and colleagues defined neurons without TH as dormant DAergic cells that survive or are bound to die at later stages [26]. Future studies are needed to assess whether these neurons will die in LPS-injected WT rats at later phases. It is also worth mentioning that a significant portion of TH^-/DCC^+ neurons was demonstrated in the SNpc of various PD animal models and post-mortem PD brains [26]. Similar results were reported on the *parkin*$^{-/-}$ mice, another PD model, after six months of repeated low-dose intraperitoneal LPS injections. Both *wild-type* and *parkin*$^{-/-}$ mice show substantial TH^+ neuronal loss, but only in LPS-treated *parkin*$^{-/-}$ mice there is a significant reduction of NeuN-positive neurons in the SNpc [33].

Another important feature highlighted in the present study is the dystrophic TH^+ dendritic arborizations, branching from SNpc surviving DAergic neurons towards the SNpr in LPS *Snca*$^{+/+}$ rats, anticipating by almost seven months similar alterations in the naïve *Snca*$^{+/+}$ animals [21]. The loss of neuronal complexity and the decreased dendritic arborization have been linked to α-synuclein overexpression in virally infected DAergic neurons *in vitro* and *in vivo*, preceding their eventual death [34,35] and resembling PD patient's post-mortem alterations [36].

The loss of DAergic neurons is associated with a greater extent of reduced evoked striatal DA release in LPS *Snca*$^{+/+}$ compared with SAL *Snca*$^{+/+}$ rats. However, no significant difference in TH immunoreactivity in the striatum was observed. In other genetic α-synuclein-based models, TH immunoreactivity in the striatum is unaltered at early phases [20,19,37] and in the *parkin*$^{-/-}$ PD model under repeated LPS administrations [38]. A possible explanation for the lack of reduction in striatal TH immunoreaction despite DAergic neuronal loss in the SNpc could be the presence of compensatory TH upregulation due to the sprouting of the surviving DAergic terminals. Besides T lymphocytes, NK cells are increased in the striatum and this could account for their neuroprotective role in PD that has been proposed based on *in vitro* and *in vivo* that suggest they might clear α-synuclein aggregates [39–43], thus protecting the surviving DAergic terminals, at least in an initial phase of pathology progression.

The increased expression of activations markers on microglia like MHC-II and CD86, which provide respectively the first and costimulatory signals necessary for T cell activation, coupled with the increased percentages of T cells in both brain areas suggest the instauration of an

immunological synapse at key areas involved in PD pathology which could drive and sustain neuroinflammation and lead to neurodegeneration.

According to our results, the decrease of DAergic neurons in the SNpc and evoked striatal DA of LPS-treated *Snca*$^{+/+}$ rats did not alter motor behavior, evaluated by rotarod and open-field tests. This result may not be surprising, because a high degree of neuronal degeneration is required for motor symptoms to be evident, in animals [37] and humans [44,45]. Similarly, the decreased DA release in LPS *Snca*$^{+/+}$ rats did not alter the preference for a sweet-tasty solution, commonly used to assess the presence of a depressive-like behavior, such as anhedonia. In a recently published work, reduced sucrose consumption has been reported shortly after systemic LPS administration [46]. However, this condition could reflect a more acute phase in response to the LPS-induced inflammatory activation.

Concluding remarks

Our data support a dual-hit hypothesis for PD, whereby elevated endotoxin under a genetic predisposition may interact or synergize, driving neurodegenerative processes that underlie PD neuropathology. We cannot discern whether the synergy between α-synuclein overexpression and LPS-induced inflammation is limited to an acceleration of PD-like symptoms typically expressed at later stages in *Snca*$^{+/+}$ rats or exacerbates their expression. Experiments performed at later stages from LPS injection are needed to clarify this issue. In conclusion, our double-hit model could be relevant to familiar forms of PD, in which the development of a PD profile may depend on the subjective exposure to risk environmental factors through inflammatory responses. More importantly, our findings provide further evidence for the role of the immune system in playing a key role in the onset and progression of PD.

MATERIAL AND METHODS

Animals

Homozygous transgenic rats (Sprague-Dawley background) overexpressing the human full-length SNCA locus under the control of the endogenous human regulatory elements (*Snca*$^{+/+}$) were used [18]. Two or three rats per cage were housed at standard conditions (23 ± 1°C room temperature, 45-60% relative humidity, 12-h light/dark cycle) with food and water ad libitum. Following species-specific behavior, red plastic tubes and paper are added to the cages. All procedures follow the guidelines on the ethical use of animals from the Council Directive of the European Communities (2010/63/EU) and were approved by the Italian Ministry of Health (Authorization N°617-2019PR). Experimental animals were obtained by crossing heterozygous males with heterozygous female rats and were confirmed as WT or *Snca*$^{+/+}$ following genotyping with quantitative PCR using DNA from ear biopsies and the primers for copy numbers of the α-synuclein transgene: SynProm-F: 5′-cgctcgagcggtaggaccgcttgttttagac-3′ and LC-SynPromR: 5′-cctctttc cacgccactatc-3′, normalized to the rat β-actin reference gene with primers: β-actin-F: 5′- agccatgtacgtagccatcca-3′ and β-actin-R: 5′-tctccggagtccatcacaatg-3′ [18,19,21].

Treatment protocol

A single dose of lipopolysaccharide (LPS) from *Escherichia coli* O111:B4 (Sigma-Aldrich, #L2630) at the concentration of 5mg/kg dissolved in sterile saline (NaCl 0.9%) was intraperitoneally (i.p.) injected in *wild-type* (WT) and *Snca*$^{+/+}$ rats at two months of age [47]. Control groups consist of a single i.p. injection of sterile saline in *Snca*$^{+/+}$ rats at the same age. Animals were randomly divided into four experimental groups.

Sickness Behavior and body weight

I.p. administration of LPS induces a sickness behavior in mice or rats [22]. In this study, sickness signs consisting of absent exploration and locomotion, curled body posture, irregular fur, piloerection, and closed eyes were evaluated in the LPS-treated and control (saline) group over time after the intraperitoneal injection of LPS, as previously described by [22,23]. Animals were individually placed in a cage and scored on a four-point scale: 0 = no signs, 1 = one sign, 2 = two signs, and 3 = three or more signs. The experimenter quantifying sickness signs was blind to

experimental and control conditions. Sickness behavior and body weight were monitored after 2 h, 18h, 24h, 42h, 48h, 72h, 96h, and 168h after the i.p. injection.

Tissue collection

Immunohistochemical and cytofluorimetric analyses were carried out on brain tissues. Animals were transcardially perfused with 1% heparin in 0.1 M sodium phosphate buffer (PB), after deep anesthesia (Rompum; 20mg/ml, 0.5 ml/kg; Bayer, and Zoletil; 100mg/ml, 0.5 ml/kg; Virbac). The brain was taken from the animal's skull, and the two hemispheres were divided into two halves along the medial sagittal line. The left hemisphere was treated for subsequent immunohistological analysis, and the right hemisphere was freshly dissected and processed for high dimensional flow cytometry. The left hemisphere was post-fixed in 4% paraformaldehyde (PFA) in phosphate buffer (PB; 0.1 M, pH 7.4) at 4 °C, and kept for 72 hours in 4% PFA and replaced every 24 hours with a fresh solution.Then, samples were rinsed three times in PB and immersed in 30% sucrose and 10% glycerol solution at 4 °C until sinking for cryoprotection. Afterward, the brains were embedded into OCT, frozen in isopentane, cooled into liquid nitrogen, and stored at -80 °C. Coronal sections (30 µm) were cut from the anterior part of the brain to the midbrain using a cryostat (Leica) at -20°C. The slices were stored at 4°C in 0.1 M PB containing 0.02% sodium azide before being further processed for immunohistochemical staining.

Dissociation of substantia nigra and striatum

After animal sacrifice, substantia nigra and striatum were collected and immersed in D-PBS with high glucose buffer at 4°C. According to the manufacturer's protocol, the tissue was immediately dissociated to single-cell suspension by enzymatic degradation and myelin removal using the adult brain dissociation kit and GentleMACS dissociator (Miltenyi Biotec.). The isolated tissues were placed in C-tubes, and a mix containing Enzyme Pand Buffer Z was added to the samples. A second mix containing Enzyme A and Buffer Y is then added, C-tubes tightly closed and attached upside down onto the sleeve of the gentleMACS Octo Dissociator with Heaters (Miltenyi Biotec.). The appropriate program 37C_ABDK_02 was run for 30 minutes, and the c-tube was detached and centrifuged to collect the sample, which was then resuspended and filtered to a 70 um MACS SmartStrainer with 10 ml of cold D-PBS with high glucose. After centrifugation at 300g for 10 minutes, the sample was resuspended in the debris removal solution, gently overlayed in cold D-PBS with high glucose and centrifuged at 3000g for 10 minutes with full acceleration brake. The two top phases were aspirated and discarded, and the sample was resuspended in cold D-PBS with

highglucose, centrifuged at 1000g for 10 minutes, and then resuspended in the staining buffer ready frcell count and flow cytometry staining.

Immunophenotyping of immune cells of substantia nigra and striatum by high dimensional flow cytometry

Cellular phenotypes were assessed using multiparametric flow cytometry panels containing markers to identify cell types and activation states. These markers allowed us to exclude all cells of no interest based on physical parameters (side and forward scatter) and to gate on specific cells of interest. For the immunophenotyping of substantia nigra and striatum, single suspension cells were stained at the cell surface in different panels with PerCP5.5-conjugated anti-CD45 (1:100, Biolegend), APC-Vio770-conjugated anti-CD11b/c (1:100, REAffinity Miltenyi Biotec.), APC-conjugated anti-CD161 (1:100, Biolegend) or CD86 (1:100, Miltenyi Biotec.), PE-conjugated anti-CD45RA (1:100, Biolegend), PE-Cy7-conjugated anti-CD3 (1:100, Miltenyi Biotec.) or anti-MHC-II (1:100, REAffinity Miltenyi Biotec.), and FITC-conjugated anti-granulocytes (1:100 Miltenyi Biotec.) or VioBright-conjugated anti-ACSA-2/O4/CD31 (1:100 REAffinity Miltenyi Biotec.) for 15 minutes at 4°C in the dark. After the staining, cells were washed and resuspended in PBS, ready to be acquired. These markers allowed us to identify the different cell populations correctly. Briefly, astrocytes, oligodendrocytes, and endothelial cells were excluded based on their expression of ACSA-2, O4, and CD31 (Lineage). The remaining cells were identified as CD45+ total leucocytes/resident immune cells. Inside this gate, microglial cells were identified as $CD45^{low}CD11b/c^{+}$ cells and infiltrated myeloid cells as $CD45^{high}CD11b^{high}$, which were subsequently identified as macrophages according to the expression of F4/80. The remaining of $CD45^{high}CD11b^{low}$ cells were further gated to identify T-lymphocytes as $CD3^{+}$, B-lymphocytes as $CD45RA^{+}$, and NK cells as $CD161^{+}$. The expression of CD68 and MHC-II was further assessed inside the microglial cell population. All samples were acquired on a 13-color Cytoflex (Beckman Coulter). For each analysis, at least $0.2x10^{6}$ live cells were acquired by gating on aqua Live/Dead negativecells and then analyzed by the Flowjo analysis software (Tree Star), as reported [48].

Immunophenotyping of immune cells of the peripheral blood by flow cytometry

Peripheral blood was collected from the animals and whole blood was lyzed with the RBC (1X) solution for 10 minutes at 37°C. Upon lysis, cells were washed and resuspended in cold PBS for immunophenotyping. Cells were stained at the cell surface with FITC-conjugated CD4 (1:100, Biolegend) or anti-agranulocytes (1:100, Miltenyi Biotec), PerCP5.5-conjugated anti-CD8 (1:100, Biolegend) or anti-CD45 (1:100, Biolegend), APC-conjugated anti-CD25 (1:80, Biolegend), PE-

conjugated anti-CD45RA (1:100, Biolegend), APC-conjugated anti- CD161 (1:100, Biolegend), PE-Vio770-conjugated anti-CD3 (1:100, REAffinity Miltenyi Biotec) and APC-Vio770-conjugated anti-CD11b/c (1:100, REAffinity Miltenyi Biotec.) for 15 minutes at 4°C in the dark. After the staining, cells were washed and incubated with a fixing solution (1:3, Biolegend) in the dark for 15 minutes at room temperature. Cells were then washed with PBS and made permeable with Cytofix/Cytoperm (1:10, Biolegend) and then stained intracellularly with APC-conjugated anti-IFN-γ (1:100, Biolegend), PE-conjugated anti-IL-17 (1:30, Biolegend) and PE-CF594-conjugated anti-FoxP3 (1:50, BD Biosciences) in Cytoperm at room temperature for 30 min. After the incubation, cells were washed and resuspended in PBS, ready to be acquired. These markers allowed us to identify the different cell populations correctly. Briefly, cells were then gated on CD45 to identify total leucocytes. Inside this gate, granulocytes were identified with their specific marker, monocytes and myeloid cells as CD11b/c$^+$, T-lymphocytes as CD3$^+$, B-lymphocytes as CD45RA$^+$ and NK cells as CD161$^+$ cells. All samples were acquired on a 13-color Cytoflex (Beckman Coulter) and for each analysis, at least 0.5x10^6 live cells were acquired by gating on aqua Live/Dead negative cells and then analyzed by the Flowjo analysis software (Tree Star), as reported [19,48,49].

Immunohistochemistry

For stereological cell count and optical density analysis, the SNpc and striatum slices were processed for chromogenic immunohistochemistry. First, the endogenous peroxidase was neutralized with a 3% H_2O_2 solution in PB. Sections were then incubated with a blocking solution made with 5% normal goat serum (NGS) and 0.3% TritonX-100 (Sigma) in a PB solution for 1h to prevent the non-specific binding of antibodies. Free-floating sections were incubated with the primary anti-TH antibody (1:1000, Millipore; #MAB318) diluted in PB containing 0.3% Triton X-100 overnight at 4°C. After three rinses, sections were incubated with a biotinylated secondary antibody (Jackson Immunoresearch Laboratories; #AP132B), followed by the incubation with extravidin-peroxidase (1:1000, Sigma; #SE2886). The antigen-antibody binding is then detected using chromogen 3,30-diaminobenzidine (DAB; Sigma). Finally, sections were dehydrated in a series of alcohols (50%, 70%, 95%, 100%), cleared in Xylene, and coverslipped with Entellan mounting medium (Sigma).

Immunofluorescence

Sections were first incubated with a blocking solution made with 5% normal donkey serum and 0.3% TritonX-100 (Sigma) in a PB solution for 1h to prevent the non-specific binding of antibodies. The primary antibodies (TH/DDC, TH/IBA1; listed in Table 1) were incubated over-weekend in PB containing 0.3% Triton X-100 at 4°C and then incubated for 2h at room temperature with the adequate secondary antibodies (listed in table 1). Sections were counterstained with DAPI (4',6-diamidin-2-fenilindolo). The specificity of the immunofluorescence labeling was confirmed by omitting primary antibodies and using normal serum instead (negative controls). Confocal laser scanner microscopy (LSM800, Zeiss, Oberkochen, Germany) was used to acquire images.

Table 1. Primary and secondary antibodies used for immunofluorescence.

Primary antibodies	**Cat. Number**	**Host**	**Dilution**	**Manufacturer**
Tyrosine hydroxylase	#MAB318	Mouse	1:1000	Millipore
IBA1	#019-19741	Rabbit	1:800	Wako
DOPA Decarboxylase	#GTX134053	Rabbit	1:800	Genetex
Secondary antibodies	**Cat. Number**	**IgG**	**Dilution**	**Company**
Alexa Fluor 488 donkey	#A21202	Mouse	1:200	Thermo Fisher Scientific
Alexa Fluor 555 donkey	#A31572	Rabbit	1:200	Thermo Fisher Scientific

Stereological cell count

The three-dimensional optical fractionator stereological probe was used to estimate the numberof TH^+ neurons in the SNpc and the Ionized calcium-binding adapter molecule 1-positive ($IBA1^+$) cells in the SNpc and striatum. We used the Stereo Investigator System (MicroBright-Field, Vermont, USA). An optical microscope (Axio Imager M2, Zeiss, Oberkochen, Germany) equipped with a motorized stage, a MAC 6000 controller (Ludl Electronic Products, Ltd) and a camera are connected to software Stereoinvestigator 2019.1.3. The region of interest was defined by TH staining and the area distinction was performed according to the rat brain Paxinos and Franklin's

atlas and outlined with a 5x objective. The three-dimensional optical fractionator stereological probe (x, y, z dimension of 50×50×30 µm, with a guard zone of 5 µm along the z axis) was used. Cells were marked with a 40x objective. All quantifications were performed by an investigator blinded to the experimental groups.

Morphological analyses of tyrosine hydroxylase fibers

Three free-floating sections (30 µm) per animal, including the dorsolateral striatum or the SNpr, were treated as for stereological cell count. Sections were photographed with a light microscope (Axio Imager M2, Zeiss, Oberkochen, Germany). Densitometric analysis (OD) of TH^+ fibers was analyzed using the Java image processing and plugin analysis program in ImageJ (NIH, USA). Densitometry values were corrected for non-specific background staining by subtracting densitometric values from the cortex for the striatum and from the surrounding neuropil for SNpr in the same images. All quantifications were performed by an investigator blinded to the experimental groups.

Sholl analysis

$IBA1^+$ cells were imaged with an optical microscope (Axio Imager M2, Zeiss, Oberkochen, Germany) equipped with a motorized stage and a camera connected to Neurolucida 2020.1.2 (MicroBright-Field, Vermont, USA) that allows for quantitative 3D analysis of the entire cell body and branching. Only cells with intact processes unobscured by background labeling or other cells were included in cell reconstruction. The cell body area and perimeter, number of intersections, number of nodes(branch points) and endings, and total length of processes were traced and exported to Neurolucida Explorer 2019.2.1 (MicroBright-Field, Vermont, USA). To account for changes in the cell's complexity concerning distance from the soma, concentric rings (radii) were spaced 10 µm apart around the cell, centered at the centroid of the cell body and radiating outward. Branching originating from the soma and the number of branch points and endings, processes intersecting the radii and process length were measured as a function of the distance from the cell soma for each

radius. Overall, fifteen cells per animal were selected randomly for analysis, and all data were subsequently averaged for each rat. All quantifications were performed by an investigator blinded to the experimental groups.

Cortico-striatal slice preparation

Acute brain slices were obtained following isoflurane anesthesia and decapitation. The brain was quickly removed, and 250–300 µm thick coronal slices containing the striatum were cut with a Leica vibratome (VT1200S) using chilled bubbled (95% O2, 5% CO2) 'sucrose-based' artificial CSF (aCSF) solution containing (in mM): KCl3, NaH_2PO_4 (1.25), $NaHCO_3$ (26), $MgSO_4$ (10), $CaCl_2$ (0.5), glucose (25), sucrose (185); ~300 mOsm, pH 7.4). Slices were used after a minimum 40 min recovery period in standard aCSF solution containing (in mM): NaCl 126, KCl 2.5, $NaH2PO_4$ (1.2), $NaHCO_3$ (24), $MgCl_2$ (1.3), $CaCl_2$ (2.4), glucose (10) (~290 mOsm, pH 7.4) at 32 °C.

Constant Potential Amperometry

Amperometric detection of electrically evoked DA release was performed in acute brain slices containing the striatum. The carbon fiber electrode was gently positioned into the tissue, and the voltage (MicroC potentiostat, World Precision Instruments) was imposed between the carbon fiber electrode and the Ag/AgCl pellet at 0.60 V. The DA-recording carbon fiber electrode (diameter 30 µm, length 100 µm, World Precision Instruments) was positioned near a bipolar Ni/Cr stimulating electrode to a depth of 50–150 µm into the coronal slice. For stimulation, a single rectangular electrical pulse was applied using a DS3 Stimulator (Digitimer) every 5 min along a range of stimulation intensities (20–1000 µA, 20–80 µs duration). Under stimulation, DA-containing vesicles were released frompresynaptic terminals. When DA molecules in the synaptic milieu hit the carbon surface, electrodes were transferred, and a current can be measured. In response to a protocol of increasing stimulation, a plateau of DA release was reached at maximal stimulation (1000 µA,80 µs). To measure changes in DA synaptic activity caused by drugs affecting the dopamine transporter (DAT) or D23 receptors, we analyzed the effects on evoked DA release by applying cocaine or quinpirole, respectively. Drugs were superfused to the striatal slice when the extracellular DA response to electrical stimulation was stable for four or five successive stimulations. The evoked release of DA was evaluated following bath perfusion of 0.3 o1 µM Cocaine dissolved in aCSF [27]. The perfusion was done for 10 minutes when the maximum effect on the DAT by cocaine was reached, and then it was washed out and followed for at least 1 h. The activity of D2 receptors on DA release was evaluated following bath perfusion of 0.03 µM quinpirole, an agonist of the D2

receptor. As for cocaine, quinpirole was perfused for 5 minutes and washed out for 30 minutes. Signals were digitized with Digidata 1440A coupled to a computer running pClamp 10 (Molecular Devices). At the end of each experiment, electrode calibration was performed by bath-perfused DA at known concentrations (0.3–10 μM).

Behavioral tests

Three months after the single injection, rats were tested for the Rotarod, open field, and sucrose preference tests.

Animals were habituated for 1 h to the testing room before the beginning of Rotarod and open field tests. At the end of each session/trial, all apparatus were cleaned with 70% ethanol to remove olfactory cues.

Rotarod test

Motor coordination and balance were tested using an accelerating Rotarod protocol (LE8355, Panlab, Spain). The apparatus consisted of a rod suspended horizontally at 47 cm from the floor. All animals were accustomed to being placed on the rod rotating at low speed (4 rpm) for at least 30 seconds before the first session of the test, which consisted of four sessions. Sessions were performed on two consecutive days (with an inter-session interval of 3.5 h) with an accelerating rod from 4 to 40 rpm in 300 s. Each session consisted of three trials, with at least 5 min of rest between trials. For each trial, the time the rat fell from the rod was recorded (maximum 300 s). The first three sessions are considered pre-training on the Rotarod apparatus to reach a stable performance. The fourth session was considered the final test, and the latency to fall from the rod was analyzed by averaging the three trial records.

Open field test

The open field is a simple test to evaluate general motor and explorative behavior inrodent models of CNS disorders. The apparatus consisted of a cylindrical plastic arena (100 cm in diameter) with dark walls (35 cm high) and floor, placed in a room with dim lighting. During the test, each animal was placed in the center of the arena and freely allowed to explore the apparatus for 10 min. Experiments were recorded with a video camera suspended above the arena, and data were analyzed with EthoVision (Noldus, The Netherlands) video tracking software, and the total distance traveled was measured.

Sucrose preference test

The sucrose preference test assesses the animal's interest in a sweet-tasting sucrose solution relative to unsweetened water. Rats were habituated to drinking from two equally accessible bottles and were singly housed for the test duration. The test cage was the same throughout the experiment. Rats were exposed to a double-choice drinking test, with the two bottles containing one sucrose solution (1%) and the other drinking water. To avoid side preference, thesucrose bottle was placed on the left for half of the cages and on the right for the othercages. Each bottle was refilled with fresh water or sucrose solution and inverted to its original position every day for two consecutive days. After 72h, the water and sucrose solution consumption was measured with a graduated cylinder. A 48h testing period allowed us to preclude any effects of neophobia, artefactual bias toward any one side, and perseveration effects. Further, it provided information regarding long-term access to a rewarding stimulus. The percentage of sucrose intake and water intake was evaluated as follows:

$$\frac{sucrose\ 1\%\ intake\ (ml)}{(sucrose 1\% + water)/kg} \times 100 \quad \text{and} \quad \frac{water\ intake\ (ml)}{(sucrose 1\% + water)/kg} \times 100$$

Statistical analysis

All statistical analysis was performed with GraphPad Prism (v8.0.1) using the appropriate statistical tests, as indicated in each figure legend. Data were checked for normality using the Shapiro-Wilk test or Kolmogorov-Smirnov test, followed by the appropriate statistical test. Values of $P \leq 0.05$ were considered to be statistically significant. All data were presented as mean ± SEM, and each point represents individual experiments.

DATA AVAILABILITY

Further information and request for resources and reagents should be directed to and will be fulfilled by the corresponding authors, Mariangela Massaro Cenere (mariangel.massarocenere@gmail.com) , and Nicola Biagio Mercuri (mercurin@med.uniroma2.it)

Full datasets can be found at Zenodo repository: 10.5281/zenodo.10581776

A detailed description of the conducted protocol is available at protocols.io repository: (DOI: dx.doi.org/10.17504/protocols.io.j8nlkoj65v5r/v1 (Private link for reviewers: https://www.protocols.io/private/EB5CE11EBE8F11EE8E330A58A9FEAC02 to be removed before publication)

AUTHOR CONTRIBUTIONS

MMC, VC, and NBM designed the experiments, MMC performed i.p. injections and sacrifices. MMC, MT, SLD, MF, CG, AM, FC, and BZ collected data and performed data analysis with feedback from EP, DC, AL, LP, NB, FRF, and VC. MMC, VC, NBM wrote and revised the manuscript. All authors contributed to the article and approved the submitted version.

FUNDING

This research was funded in whole or in part by Aligning Science Across Parkinson's 020505 through the Michael J. Fox Foundation for Parkinson's Research (MJFF). For the purpose of open access, the author has applied a CC BY 4.0 public copyright license to all Author Accepted Manuscripts arising from this submission. Conducted work was also supported by NEXTGENERATIONEU (NGEU) and funded by the Ministry of University and Research (MUR), National Recovery and Resilience Plan (NRRP), project MNESYS (PE0000006) – A Multiscale integrated approach to the study of the nervous system in health and disease (DN. 1553 11.10.2022), and by the Ministry of University and Research (MIUR) - PRIN (Bando 2017, Prot. 2017ENN4FY, N.B.M).

CONFLICT OF INTEREST

The authors report no competing interests.

REFERENCES

1. Dorsey, E. R. *et al.* Global, regional, and national burden of Parkinson's disease, 1990–2016: a systematic analysis for the Global Burden of Disease Study 2016. *The Lancet Neurology* **17**, 939–953 (2018).
2. Hoehn, M. M. Parkinsonism: onset, progression, and mortality.
3. Jellinger, K. A. Neuropathobiology of non-motor symptoms in Parkinson disease. *J Neural Transm* **122**, 1429–1440 (2015).
4. Bernheimer, H., Birkmayer, W., Hornykiewicz, O., Jellinger, K. & Seitelberger, F. Brain dopamine and the syndromes of Parkinson and Huntington Clinical, morphological and neurochemical correlations. *Journal of the Neurological Sciences* **20**, 415–455 (1973).
5. Spillantini, M. G. *et al.* α-Synuclein in Lewy bodies. *Nature* **388**, 839–840 (1997).
6. Spillantini, M. G., Crowther, R. A., Jakes, R., Hasegawa, M. & Goedert, M. α-Synuclein in filamentous inclusions of Lewy bodies from Parkinson's disease and dementia with Lewy bodies. *Proc Natl Acad Sci U S A* **95**, 6469–6473 (1998).
7. Nalls, M. A. *et al.* Identification of novel risk loci, causal insights, and heritable risk for Parkinson's disease: a meta-analysis of genome-wide association studies. *The Lancet Neurology* **18**, 1091–1102 (2019).
8. Singleton, A. & Hardy, J. Progress in the genetic analysis of Parkinson's disease. *Human Molecular Genetics* **28**, R215–R218 (2019).
9. Tansey, M. G. *et al.* Inflammation and immune dysfunction in Parkinson disease. *Nat Rev Immunol* **22**, 657–673 (2022).
10. Wijeyekoon, R. S. *et al.* Peripheral innate immune and bacterial signals relate to clinical heterogeneity in Parkinson's disease. *Brain Behav Immun* **87**, 473–488 (2020).
11. Brown, G. C., Camacho, M. & Williams-Gray, C. H. The Endotoxin Hypothesis of Parkinson's Disease. *Movement Disorders* **38**, 1143–1155 (2023).
12. Qin, L. *et al.* Systemic LPS causes chronic neuroinflammation and progressive neurodegeneration. *Glia* **55**, 453–462 (2007).

13. Liu, Y. *et al.* Endotoxin induces a delayed loss of TH-IR neurons in substantia nigra and motor behavioral deficits. *NeuroToxicology* **29**, 864–870 (2008).
14. Zheng, H.-F. *et al.* Autophagic Impairment Contributes to Systemic Inflammation-Induced Dopaminergic Neuron Loss in the Midbrain. *PLOS ONE* **8**, e70472 (2013).
15. Bodea, L.-G. *et al.* Neurodegeneration by Activation of the Microglial Complement–Phagosome Pathway. *J. Neurosci.* **34**, 8546–8556 (2014).
16. Beier, E. E. *et al.* Alternative microglial activation is associated with cessation of progressive dopamine neuron loss in mice systemically administered lipopolysaccharide. *Neurobiology of Disease* **108**, 115–127 (2017).
17. Gasparotto, J. *et al.* Systemic Inflammation Changes the Site of RAGE Expression from Endothelial Cells to Neurons in Different Brain Areas. *Mol Neurobiol* **56**, 3079–3089 (2019).
18. Nuber, S. *et al.* A progressive dopaminergic phenotype associated with neurotoxic conversion of α-synuclein in BAC-transgenic rats. *Brain* **136**, 412–432 (2013).
19. Krashia, P. *et al.* Blunting neuroinflammation with resolvin D1 prevents early pathology in a rat model of Parkinson's disease. *Nat Commun* **10**, 3945 (2019).
20. Polissidis, A. *et al.* Psychosis-Like Behavior and Hyperdopaminergic Dysregulation in Human α-Synuclein BAC Transgenic Rats. *Movement Disorders* **36**, 716–728 (2021).
21. Ledonne, A. *et al.* Morpho-Functional Changes of Nigral Dopamine Neurons in an α-Synuclein Model of Parkinson's Disease. *Mov Disord* **38**, 256–266 (2023).
22. Dantzer, R. Cytokine-Induced Sickness Behavior: Where Do We Stand? *Brain, Behavior, and Immunity* **15**, 7–24 (2001).
23. Flores-Martinez, Y. M. *et al.* Acute Neuroinflammatory Response in the Substantia Nigra Pars Compacta of Rats after a Local Injection of Lipopolysaccharide. *J Immunol Res* **2018**, 1838921 (2018).
24. Lauritsen, J. & Romero-Ramos, M. The systemic immune response in Parkinson's disease: focus on the peripheral immune component. *Trends in Neurosciences* **46**, 863–878 (2023).
25. Sulzer, D. *et al.* T cells of Parkinson's disease patients recognize α–synuclein peptides. *Nature* **546**, 656–661 (2017).

26. Heo, J. Y. *et al.* Aberrant Tonic Inhibition of Dopaminergic Neuronal Activity Causes Motor Symptoms in Animal Models of Parkinson's Disease. *Current Biology* **30**, 276-291.e9 (2020).
27. Federici, M. *et al.* Paradoxical Abatement of Striatal Dopaminergic Transmission by Cocaine and Methylphenidate. *J Biol Chem* **289**, 264–274 (2014).
28. Stuchlik, A., Rehakova, L., Rambousek, L., Svoboda, J. & Vales, K. Manipulation of D2 receptors with quinpirole and sulpiride affects locomotor activity before spatial behavior of rats in an active place avoidance task. *Neuroscience Research* **58**, 133–139 (2007).
29. Kelly, M. A. *et al.* Locomotor Activity in D2 Dopamine Receptor-Deficient Mice Is Determined by Gene Dosage, Genetic Background, and Developmental Adaptations. *J. Neurosci.* **18**, 3470–3479 (1998).
30. Gao, H.-M. *et al.* Neuroinflammation and α-synuclein dysfunction potentiate each other, driving chronic progression of neurodegeneration in a mouse model of Parkinson's disease. *Environ Health Perspect* **119**, 807–814 (2011).
31. Contaldi, E., Magistrelli, L. & Comi, C. T Lymphocytes in Parkinson's Disease. *Journal of Parkinson's Disease* **12**, S65–S74 (2022).
32. Brochard, V. *et al.* Infiltration of CD4+ lymphocytes into the brain contributes to neurodegeneration in a mouse model of Parkinson disease. *J Clin Invest* **119**, 182–192 (2009).
33. Bido, S. *et al.* Microglia-specific overexpression of α-synuclein leads to severe dopaminergic neurodegeneration by phagocytic exhaustion and oxidative toxicity. *Nat Commun* **12**, 6237 (2021).
34. Dagra, A. *et al.* α-Synuclein-induced dysregulation of neuronal activity contributes to murine dopamine neuron vulnerability. *npj Parkinsons Dis.* **7**, 1–22 (2021).
35. Decressac, M., Mattsson, B., Lundblad, M., Weikop, P. & Björklund, A. Progressive neurodegenerative and behavioural changes induced by AAV-mediated overexpression of α-synuclein in midbrain dopamine neurons. *Neurobiology of Disease* **45**, 939–953 (2012).
36. Cheng, H.-C., Ulane, C. M. & Burke, R. E. Clinical progression in Parkinson disease and the neurobiology of axons. *Ann Neurol* **67**, 715–725 (2010).

37. Wegrzynowicz, M. *et al.* Depopulation of dense α-synuclein aggregates is associated with rescue of dopamine neuron dysfunction and death in a new Parkinson's disease model. *Acta Neuropathol* **138**, 575–595 (2019).

38. Frank-Cannon, T. C. *et al.* Parkin Deficiency Increases Vulnerability to Inflammation-Related Nigral Degeneration. *J. Neurosci.* **28**, 10825–10834 (2008).

39. Vivier, E., Tomasello, E., Baratin, M., Walzer, T. & Ugolini, S. Functions of natural killer cells. *Nat Immunol* **9**, 503–510 (2008).

40. Earls, R. H. & Lee, J.-K. The role of natural killer cells in Parkinson's disease. *Exp Mol Med* **52**, 1517–1525 (2020).

41. Earls, R. H. *et al.* NK cells clear α-synuclein and the depletion of NK cells exacerbates synuclein pathology in a mouse model of α-synucleinopathy. *Proceedings of the National Academy of Sciences* **117**, 1762–1771 (2020).

42. Earls, R. H. *et al.* Intrastriatal injection of preformed alpha-synuclein fibrils alters central and peripheral immune cell profiles in non-transgenic mice. *Journal of Neuroinflammation* **16**, 250 (2019).

43. Weiss, F., Labrador-Garrido, A., Dzamko, N. & Halliday, G. Immune responses in the Parkinson's disease brain. *Neurobiology of Disease* **168**, 105700 (2022).

44. BROOKS, D. J. *et al.* THE RELATIONSHIP BETWEEN LOCOMOTOR DISABILITY, AUTONOMIC DYSFUNCTION, AND THE INTEGRITY OF THE STRIATAL DOPAMINERGIC SYSTEM IN PATIENTS WITH MULTIPLE SYSTEM ATROPHY, PURE AUTONOMIC FAILURE, AND PARKINSON'S DISEASE, STUDIED WITH PET. *Brain* **113**, 1539–1552 (1990).

45. Kordower, J. H. *et al.* Disease duration and the integrity of the nigrostriatal system in Parkinson's disease. *Brain* **136**, 2419–2431 (2013).

46. Zhang, J. *et al.* LPS activates neuroinflammatory pathways to induce depression in Parkinson's disease-like condition. *Frontiers in Pharmacology* **13**, (2022).

47. Ramírez Dds, MSc, PhD, K., Quesada-Yamasaki Mls, D. & Fornaguera-Trías PhD, J. A Protocol to Perform Systemic Lipopolysacharide (LPS) Challenge in Rats. *Odovtos - Int J Dent Sc* **21**, 53–66 (2019).

48. Sciarretta, F. *et al.* Lipocalin-2 promotes adipose–macrophage interactions to shape peripheral and central inflammatory responses in experimental autoimmune encephalomyelitis. *Molecular Metabolism* **76**, 101783 (2023).

49. Turchi, R. *et al.* Butyrate prevents visceral adipose tissue inflammation and metabolic alterations in a Friedreich's ataxia mouse model. *iScience* **26**, 107713 (2023).

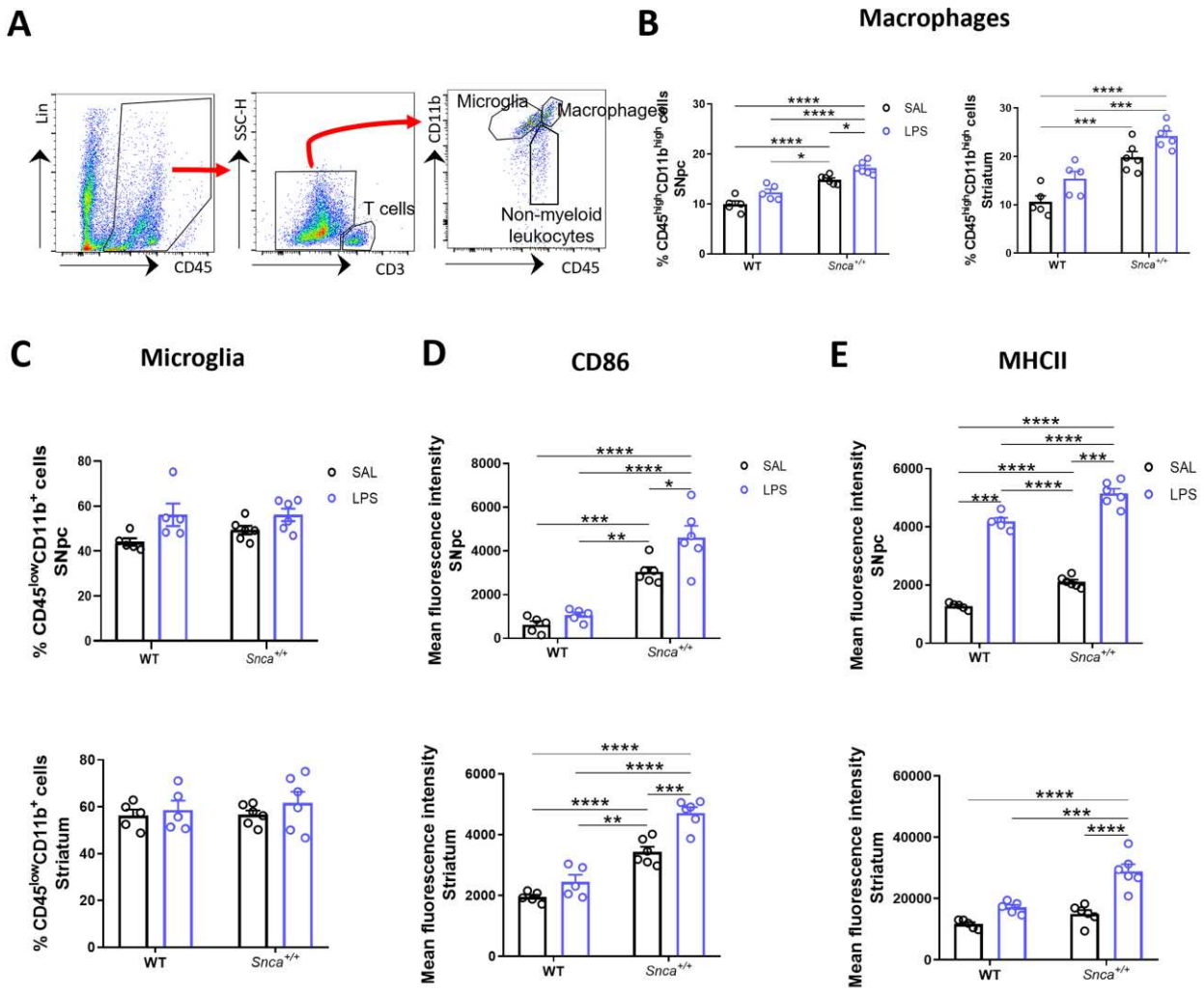

Figure 1. LPS-induced monocyte infiltration and microglial activation in CNS. A) Representative flow cytometry dot plots of isolated brain cells illustrating the gating strategy to determine profiles based on $CD45^{low}CD11b^{+}$ for microglia, $CD45^{high}CD11b^{high}$ macrophages for the central nervous system (CNS)-associated phagocytes, and $CD45^{high}CD11b^{-}$ cells. **B)** Percentage of $CD45^{high}CD11b^{high}$ cells in the SNpc (left) and in the striatum (right). Error bars represent ±SEM. (n=5/6 rats/group; Ordinary two-way ANOVA for Genotype vs Treatment; SNpc: Interaction, $F(1, 18) = 0.003483$, Genotype, $F(1, 18) = 79.06$, $p<0.001$, Treatment, $F(1, 18) = 18.48$, $p<0.0001$; *$p<0.05$, ****$p<0.0001$, with Bonferroni's *post hoc* multiple comparisons test; striatum: Interaction, $F(1, 18) = 0.02436$, Genotype, $F(1, 18) = 52.37$, $p<0.0001$ Treatment, $F(1, 18) = 13.76$, $p<0.01$; ***$p<0.001$, ****$p<0.0001$, with Bonferroni's *post hoc* multiple comparisons test). **C)** Percentage of $CD45^{low}CD11b^{+}$ microglia in the SNpc (top) and in the striatum (bottom). Error bars represent ±SEM. (n=5/6 rats/group, Ordinary two-way ANOVA for Genotype vs Treatment; SNpc: Interaction, $F(1, 18) = 0.7841$, Genotype, $F(1, 18) = 0.7550$, Treatment, $F(1, 18) = 9.796$, $p<0.01$; striatum: Interaction, $F(1, 18) = 0.1473$). **D)** Mean fluorescence of CD86 both in the SNpc (top) and striatum (bottom). (n=5/6 rats/group; Ordinary two-way ANOVA for Genotype vs Treatment; SNpc: Interaction, $F(1, 18) = 2.858$, Genotype, $F(1, 18) = 79.88$, $p<0.0001$, Treatment, $F(1, 18) = 9.063$, $p<0.001$; *$p<0.05$, **$p<0.01$, ***$p<0.001$, ****$p<0.0001$, with Bonferroni's *post hoc* multiple comparisons test; striatum: Interaction, $F(1, 18) = 4.848$, $p<0.05$, Genotype, $F(1, 18) = 111.9$, $p<0.0001$, Treatment, $F(1, 18) = 25.47$, $p<0.0001$; **$p<0.01$, ***$p<0.001$, ****$p<0.0001$, with Bonferroni's *post hoc* multiple comparisons test). **E)** Mean fluorescence of MHC-II both in the SNpc (top) and striatum (bottom). (n=5/6 rats/group; Ordinary two-way ANOVA for Genotype vs Treatment; SNpc: Interaction, $F(1, 18) = 0.2921$, Genotype, $F(1, 18) = 56.27$, $p<0.0001$, Treatment, $F(1, 18) = 623.2$, $p<0.0001$; ***$p<0.001$, ****$p<0.0001$, with Bonferroni's *post hoc* multiple comparisons test; striatum: Interaction, $F(1, 18) = 7.674$, $p<0.05$, Genotype, $F(1, 18) = 24.36$, $p<0.001$, Treatment, $F(1, 18) = 40.04$, $p<0.0001$; ***$p<0.001$, ****$p<0.0001$, with Bonferroni's *post hoc* multiple comparisons test).

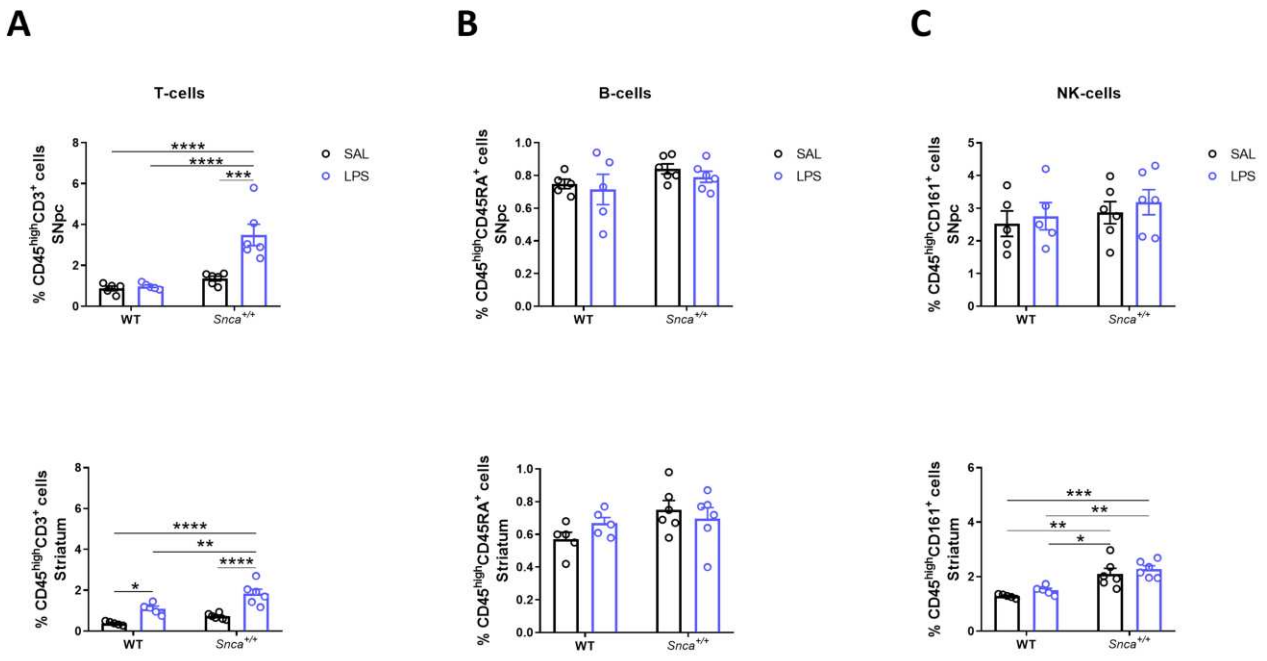

Figure 2. Infiltrating peripheral immune cells into the SN and striatum 3 months after LPS administration in *Snca*$^{+/+}$ rats. A) Bar plots of the percentage of CD45^{high}CD3^{+} T cells in the SNpc (top) and striatum (bottom). (n=5/6 rats/group; Ordinary two-way ANOVA for Genotype vs Treatment; SNpc: Interaction, F (1, 18) = 11.58, p<0.01, Genotype, F (1, 18) = 25.14, p<0.0001, Treatment, F (1, 18) = 14.07, p<0.01; ***p<0.001, ****p<0.0001, with Bonferroni's *post hoc* multiple comparisons test; striatum: Interaction, F (1, 18) = 2.041, Genotype, F (1, 18) = 15.05, p<0.01, Treatment, F (1, 18) = 44.63, p<0.0001; *p<0.05, **p<0.01, ****p<0.0001, with Bonferroni's *post hoc* multiple comparisons test). **B)** Bar plots of the percentage of CD45^{high}CD45RA^{+} B cells in the SNpc (top) and striatum (bottom). (n=5/6 rats/group; Ordinary two-way ANOVA for Genotype vs Treatment; SNpc: Interaction, F (1, 18) = 0.02012; striatum: Interaction, F (1, 18) = 1.916). **C)** Bar plots of the percentage of CD45^{high}CD161^{+}NK cells in the SNpc (top), while, in the striatum (bottom), a significant genotype effect in *Snca*$^{+/+}$ compared to WT groups is shown, independent from treatment. (n=5/6 rats/group; Ordinary wo-way ANOVA for Genotype vs Treatment; SNpc: Interaction F (1, 18) = 0.01421; striatum: Interaction, F (1, 18) = 0.01596, Genotype, F (1, 18) = 33.17, p<0.0001, Treatment, F (1, 18) = 2.033; *p<0.05, **p<0.01, ***p<0.001, with Bonferroni's *post hoc* multiple comparisons test).

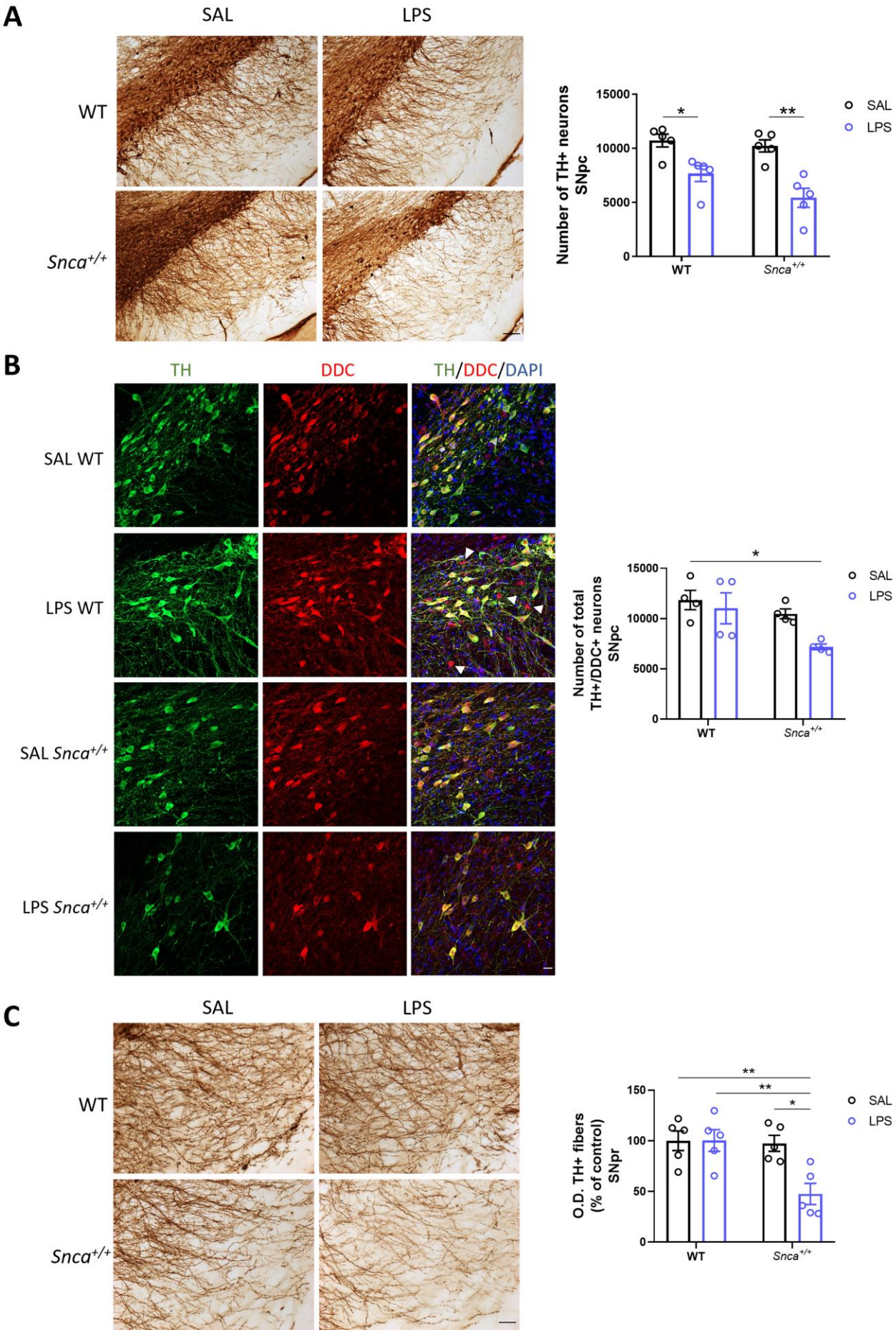

Figure 3. LPS-induced morphological alterations in SNpc. A) Left, representative coronal images of SN slices from 3,3'-diaminobenzidine (DAB)-stained TH^+ neurons in WT and *Snca*$^{+/+}$ rats treated with saline (SAL) or Lipopolysaccharide (LPS) at 3 months after injection (scale: 100µm). Right, unbiased stereological TH^+ cell count plot in the SNpc. Each point represents actual values ±SEM. (n=5 rats/group; Kruskal-Wallis test: $p<0.01$; *$p<0.05$, **$p<0.01$, with Mann Whitney test). **B)** Left, representative confocal images of stained SNpc sections for TH (green) and DDC (red) dopaminergic markers and DAPI (blue) in WT and *Snca*$^{+/+}$ rats treated with saline (SAL) or Lipopolysaccharide (LPS) at 3 months after injection (scale: 20µm). White arrowheads show TH^-/DDC^+ neurons (red). Right, unbiased stereological count of total TH^+/DDC^+ neurons in SNpc. Each point represents actual values ±SEM. (n=4 rats/group; Ordinary two-way ANOVA for Genotype vs Treatment, Interaction, $F(1, 12) = 1.675$, Genotype, $F(1, 12) = 7.522$, Treatment, $F(1, 12) = 4.677$, $p<0.05$; *$p<0.05$, with Bonferroni's *post hoc* multiple comparison test). Right bottom, magnification showing a representative image of TH^-DDC^+ neuron in an LPS WT rat. **C)** Representative image (left) and densitometric analysis (right) of coronal midbrain slice from DAB-stained TH^+ neurons in WT and *Snca*$^{+/+}$ rats treated with SAL or LPS (scale: 50µm). The values are expressed as means of each animal normalized to the total mean value of SAL WT group ± SEM. (n=5 rats/group; Ordinary two-way ANOVA for Genotype vs Treatment, Interaction, $F(1, 16) = 6.614$, $p<0.05$, Genotype, $F(1, 16) = 8.053$, $p<0.05$, Treatment, $F(1, 16) = 6.497$, $p<0.05$; *$p<0.05$, **$p<0.01$, with Bonferroni's *post hoc* multiple comparison test).

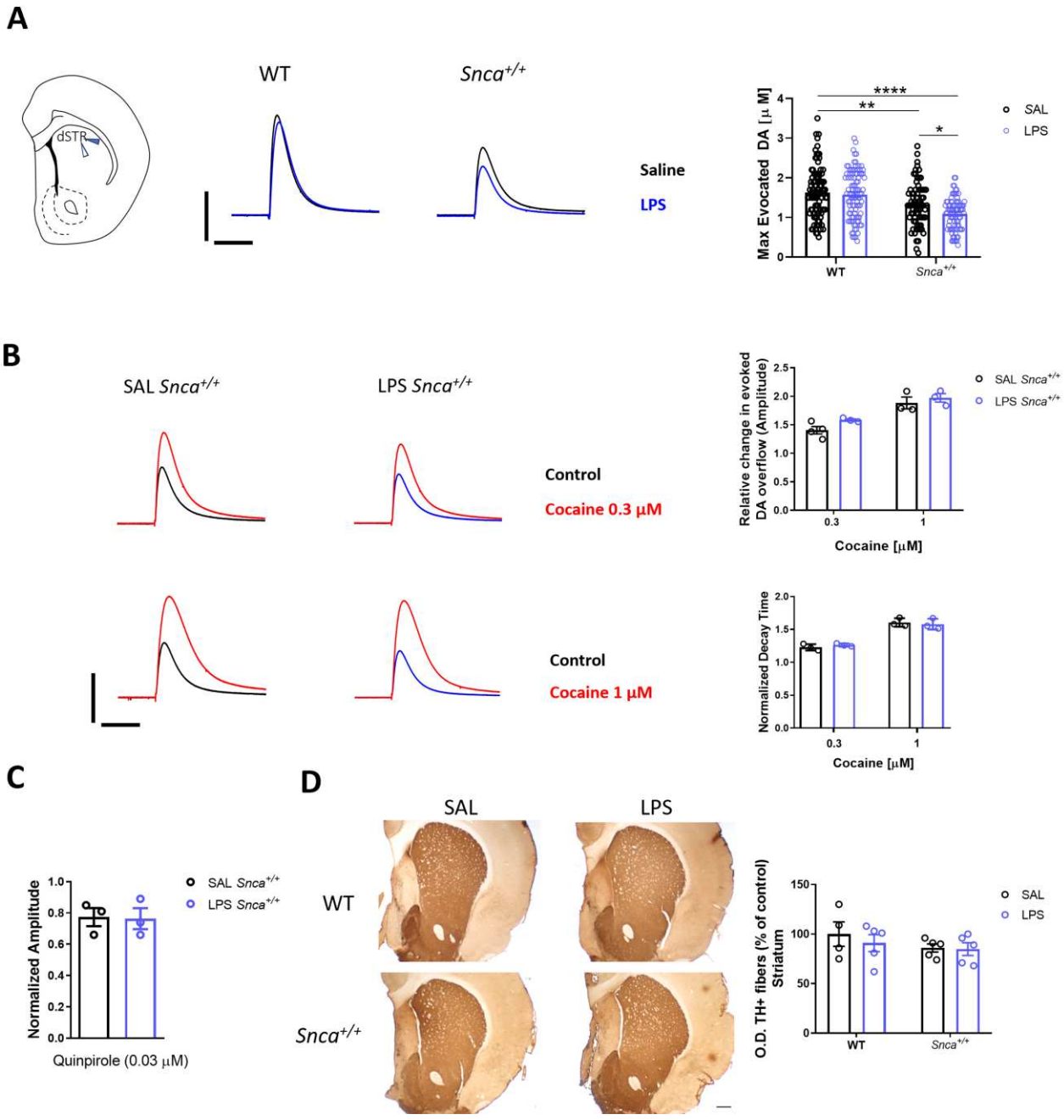

Figure 4. LPS-induced functional and morphological alterations in striatum. A) Left, schematic representation showing the placement of the stimulating (blue arrowhead) and carbon fiber (white arrowhead) used for the recordings in the dorsal striatum. Middle, representative traces (scale: 100 pA; 500 ms) and evoked DA concentration in the dorsal striatum at 3 months after treatment in WT and *Snca*$^{+/+}$ rats recorded with constant potential amperometry. Right, bar plot showing max evoked DA outflow in *Snca*$^{+/+}$ rats. (Ordinary two-way ANOVA Genotype vs Treatment; Interaction, F (1, 343) = 2.395, Genotype, F (1, 343) = 41.03, p<0.0001, Treatment, F (1, 343) = 5.763, p<0.05; *p<0.05, **p<0.01, ****p<0.0001, with Tukey's *post hoc* multiple comparisons test). **B)** Left, representative traces showing the effects of cocaine at different concentrations (top: 0.3µM; Bottom: 1µM) in SAL (left) and LPS (right) *Snca*$^{+/+}$ rats. At the top right, the bar plot indicates the effect of cocaine on DA overflow (n= 3/4 rats/group; Ordinary two-way ANOVA Treatment vs Cocaine concentrations; Interaction, F (1, 9) = 0.3939). On the right bottom, the bar plot indicates the effect of cocaine on the decay phase of the DAergic signal. Data are presented as mean ± SEM. (n= 3/4 rats/group; Ordinary two-way ANOVA Treatment vs Cocaine concentrations; Interaction, F (1, 9) = 0.1171). **C)** The bar plot shows the change in striatal DA release upon 5 min superfusion of quinpirole. Data are presented as mean ± SEM. (n= 3/4 rats/group; *t*-test, t=0.1126, P>0.05). **D)** Representative images of TH immunoreactivity of striatal coronal sections in WT and *Snca*$^{+/+}$ rats treated with SAL or LPS 3 months after treatment (scale bar: 500 µm). The values are expressed as means of each animal normalized to the total mean value of SAL WT group ± SEM. (n=5 rats/group; Ordinary two-way ANOVA for Genotype vs Treatment; Interaction, F (1, 15) = 0.2409).